Associative polymers. Part III: Shear rheology from molecular dynamics

J. Castillo-Tejas [a,*], O. Castrejón-González [b], S. Carro [a], V. González-Coronel [c], J.F.J. Alvarado [b], O. Manero [d]

[a] *Facultad de Ciencias Básicas, Ingeniería y Tecnología, Universidad Autónoma de Tlaxcala, Calzada Apizaquito S/N, Apizaco, Tlaxcala 90300, Mexico*
[b] *Departamento de Ingeniería Química, Instituto Tecnológico de Celaya, Avenida Tecnológico y García Cubas S/N, Celaya, Guanajuato 38010, Mexico*
[c] *Facultad de Ingeniería Química, Benemérita Universidad Autónoma de Puebla, Av. San Claudio y 18 Sur S/N, Puebla 72580, Mexico*
[d] *Instituto de Investigaciones en Materiales, Universidad Nacional Autónoma de México, Ciudad Universitaria, D.F. 04510, Mexico*

HIGHLIGHTS

- Shear flow is generated using a non-equilibrium molecular dynamics.
- System consists of chains with hydrophobic sites, immersed in solvent particles.
- Position of hydrophobic sites (HS) in molecule defines the viscoelastic behavior.
- HS at the end of the chain generate a highly elastic and viscous system.
- HS along the chain generate a topological restriction for associative interactions.

GRAPHICAL ABSTRACT
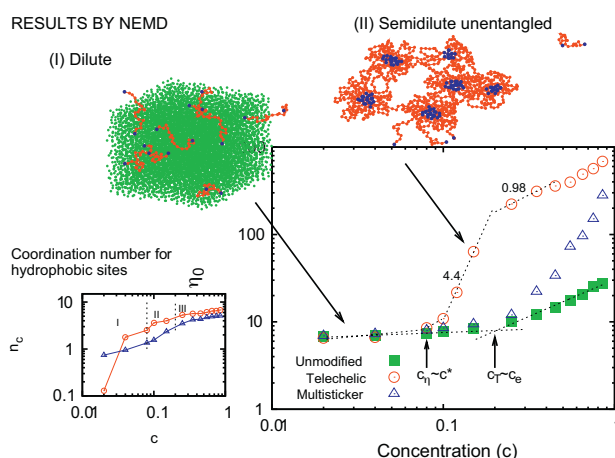
ARTICLE INFO

ABSTRACT

In this work, non-equilibrium molecular dynamics (NEMD) is used to simulate simple shear flow of associative polymer solutions of the telechelic and multi-sticker types. The objective of the work is the analysis of the effect of the hydrophobic groups of these polymers on the rheological behavior of the system. To generate the flow, the equations of motion are coupled to boundary conditions of Lees and Edward [A.W. Lees, S.F. Edward, J. Phys. C 5 (1972) 1921], where simulations are performed at constant temperature under a coarse-grain simulation scale. Three concentration regimes are identified: dilute, semi-dilute unentangled and semi-dilute entangled. In the dilute regime, the multi-sticker polymers exhibit a Newtonian constant-viscosity region, while in telechelic polymers a shear-thickening region is observed. In this regime, the molecules are isolated, so that the majority of hydrophobic interactions occur between sites of the same chain. Coordination number reveals the presence of a transient first-layer of hydrophobic neighbors, associated with the viscosity of the polymer. In the semi-dilute unentangled regime, both types exhibit a Newtonian region at low shear-rates followed by shear thinning.

* Corresponding author.
  E-mail addresses: jorge.castillo@uatx.mx, j_castillo_tejas@hotmail.com (J. Castillo-Tejas).

For telechelic polymers, the Newtonian viscosity increases with concentration with a slope of 4.4, attributed to the formation of non-isotropic aggregates with viscoelasticity levels of two orders of magnitude larger than those of the non-modified polymers. Static structure-factor suggests an increasing alignment of the multi-sticker polymer along the *x*-direction, revealing larger molecular mobility and lower viscosity than in the telechelic polymers. Finally, these results reveal that when the hydrophobic groups are located at the extremes of the polymer chain (telechelic type), the rheological behavior is strongly affected in the dilute regime by the formation of inter-connected aggregates. On the other hand, when the hydrophobic groups are located in the interior of the chain (multi-sticker type) hydrophobic associations are inhibited by topological restrictions, and in this case the viscoelastic response is only observed in the semi-dilute regime.

1. Introduction

This analysis comprises the third part of an investigation related to the rheological characterization of associative polymer solutions, namely *telechelic and multi-sticker* molecules embedded in a Newtonian fluid (the solvent). Non-equilibrium molecular dynamics simulations within a coarse-grain scale are used to simulate a rectilinear simple shear flow. Most of this work analyzes the dependency of the zero-shear viscosity (η_0) on solution concentration (c) and the viscoelastic behavior of the solutions at each concentration regime.

The rheological behavior of associative polymers has been given ample attention, in part because of the application of these polymers in important industries such as the coating, paint, water-treatment ones, and in operations for enhanced oil-recovery. Essentially, these polymers consist of a long hydrophilic macromolecular backbone, to which small hydrophobic groups are incorporated. In aqueous solution, upon increasing concentration above the critical aggregation concentration (C_g), the number of aggregates is increased, while maintaining their size and shape. Numerous studies have established that the attractive and repulsive interactions among the components in the system control and define their physical behavior. For associative polymers, interactions between hydrophobic sites define aggregates formation, and consequently, the system's behavior. If the energy of inter-action among the hydrophobic groups is 10 times the thermal energy $\sim k_B T$, associations are strong enough to affect the rheological response of the solution, otherwise the behavior would be that of an unmodified polymer. It is important to note that the aggregates are not permanent; they undergo in a constant process of breaking-reformation caused by the thermal motion and flow [1]. When intermolecular hydrophobic-interactions are strong enough, the system behaves like a gel. Experimental techniques like fluorescence, static light scattering, dynamic calorimetric, electron paramagnetic resonance and nuclear magnetic resonance have been used to study the process of aggregation [2,3].

The dynamic response of associative polymers, as revealed by rheological measurements, is that of a viscoelastic liquid and depends on two types of interactions: those due to entanglements and those caused by the topology of the hydrophobic associations. For *telechelic polymers*, Tanaka and Toga [4] mentioned that the interactions between the hydrophobic sites can lead up to six concentration-dependent conformations including open-isolated chains, isolated closed-loops, clusters of closed-loops forming micellar flowers, bridging-chains between flowers, dangling-chains and dangling-loops in clusters. Winnik et al. [5], Tripathi et al. [6] and Pellens et al. [7] describe these conformations in detail. These results motivated the implementation of a configurational analysis to verify the formation of these microstructures and their response under flow. Chassenieux et al. [8] pointed out that at high concentrations, a network of micellar flowers inter-connected by bridges is present, such that the viscosity of the system depends on the lifetime of the bridges [9–11]. The Maxwell model describes the rheological response of these polymers, which generally exhibit a single relaxation time [12,13], and in special cases, two relaxation times are found [14]. The relaxation mechanism is related to the dissociation of hydrophobic sites [5,11,15]. Under simple-shear flow, the telechelic polymers exhibit three flow regions: Newtonian, shear-thickening and shear-thinning [11–13]. It is noteworthy that the shear-thickening region is not necessarily present in the multi-sticker associative polymers [16], and in the telechelic ones, it is associated with the stretching experienced by the bridges between the micellar flowers [17–19].

For *multi-sticker polymers*, Jiménez-Regalado et al. [20] describe conformations resulting from the intra-molecular and inter-molecular hydrophobic-sites interactions. Depending on solution concentration, a chain can be isolated as their hydrophobic sites do not interact with each other, or free, when only one of the hydrophobic sites has been associated. A chain can also form an intra-chain bound conformations (knot type) when the hydrophobic sites of the same chain interact. Finally, upon increasing concentration, the inter-molecular and intra-molecular interactions generate a cross-linked system [8,20–23]. The rheological characterization of such polymers [9,24] reveals the presence of three concentration regimes: (i) dilute, wherein the viscosity is controlled by intra-molecular interactions, (ii) semi-dilute unentangled, characterized by inter-molecular hydrophobic-associations without entanglements, and (iii) semi-dilute entangled, wherein the dynamic response of the system depends on the elasticity of the hydrophobic associations and entanglement-density. Recently, Caputo et al. [25] found that in the third regime, the elasticity of the multi-sticker polymers depends strongly on the hydrophobic associations. In particular, the rheological response of these associative polymers has shown that the relaxation process is quite complex [26], involving a distribution of relaxation times [27–29].

Molecular simulations have been used to analyze the structural and equilibrium properties of associative polymers. Aggregate-formation predictions have been shown to be consistent with experimental observations in associative polymers [30] and worm-like micelles [31–33]. The strength of interactions between the hydrophobic sites, modulated with temperature, define the aggregate-type process in telechelic associative polymers [34–37], as in multi-sticker polymer solutions [38]. Using Monte-Carlo simulations, the distribution of hydrophobic sites and the strength of interactions along the chain have been shown to be important factors in the aggregation process [39,40].

Molecular dynamics simulations have shown the effect of the flow on the formation of aggregates in wormlike micelles [31,41,33] and associative polymers [42]. Under shear flow conditions, the average size of the linear micelles diminishes with shear rate [31,41]. Also, the micelles maintain their molecular conformations at low strains rate, but it is observed alignments of wormlike

micelles in flow direction and shear-banding flow at higher strains [33]. For associative polymers, molecular dynamics simulations by Khalatur et al. [42] revealed that the most chains adopt the form of a closed-loop or a stretched-conformation, but under the shear forces, the fraction of loop-like chains decreases while the fraction of bridged-chains between aggregates increases. Manassero and Castellano [43] predicted that in equilibrium, a reversible-aggregated network interconnected by bridges is present, which is broken under shear-strain. Subsequent studies demonstrated that the topology of bridges between aggregates is an important factor related to the onset of shear-thinning or shear-thickening behavior [44,45]. Using Brownian dynamics, Cass et al. [46] predicted the aggregate-formation and viscosity variation in an ample concentration range, which is consistent with experimental observations.

In general, the viscoelastic response of telechelic and multi-sticker associative polymers differ, since they have different relaxation and thickening mechanisms. In this work, non-equilibrium molecular dynamics within a coarse-grain scale is used to simulate a simple shear flow of associative polymer solutions. The hydrophobic modifications of the associative polymer molecule include the telechelic type, with the hydrophobic groups positioned at the extremes of the chain, and the multi-sticker type, with hydrophobic groups located along the chain. In this regard, the objective of this study is the analysis of the rheological response of associative polymers, on the basis of the conformations that the molecule and microstructure adopt along the characteristic concentration regimes. The relevant results of this work include a qualitative, and in some cases quantitative agreement with experiments. This analysis aims to improve the understanding of the structure and molecular conformation that defines the viscoelastic behavior of these complex fluids.

2. Theory and simulation method

2.1. Systems under study

In this paper, three types of polymer solutions are studied: (1) unmodified, (2) telechelic and (3) multi-sticker, at a reduced temperature and number density of 1.5 and 1.0, respectively. The reduced density (ρ) is defined as the ratio of the total number of sites and the volume of the simulation. Density is fixed on the basis that the system is in the liquid state (measured in terms of the radial distribution function). This density value has already been fixed in previous studies of molecular dynamics for polymer solutions and melts [47,48].

Each system under study consists of M linear molecules and S solvent particles, where each molecule is made up of twenty interlinked sites. The total number of sites (N) is given by $20M + S$ and in all simulations $N = 8000$. Simulations were developed considering an interval of concentration per site (c) of 0.02–0.85, where c is defined as the ratio of the number of sites of chain molecules and the number of total sites. In Fig. 1 a schematic representation of each solution of linear molecules is shown (including the unmodified polymer), such that in the telechelic polymer the hydrophobic groups are positioned at the beginning and end of the chain, and in the multi-sticker polymer they are placed in sites 7 and 14.

2.2. Functional form of intermolecular potential.

In molecular dynamics simulations, particles in the system interact according to the laws of classical mechanics. The total energy of the configuration is given mainly by the sum of the energies between pairs of particles:

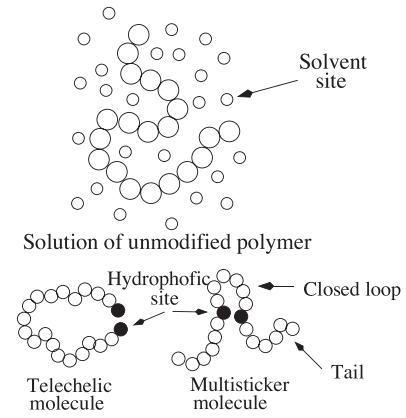$$U\left(\mathbf{r}^N\right) = \Sigma_i \Sigma_{ji} U(r_{ij}) \tag{1}$$

Fig. 1. Schematic representation of unmodified and associative polymer solutions.

where $U(\mathbf{r}^N)$ is the energy configuration and $U(r_{ij})$ is the energy resulting from the interaction between two pairs of particles i and j, which are separated by a distance r_{ij}. The force acting on a particle is obtained from the gradient of the potential function:

$$\boldsymbol{F}_i = -\nabla U\left(r_{ij}\right) \tag{2}$$

In this work, the 8000 sites in each system interact via the Lennard-Jones potential, which is truncated and smoothed at a cutting radius of $r_c = 2.5\sigma$, according to:

$$U\left(r_{ij}\right) = U_{LJ}\left(r_{ij}\right) - (r - r_c)\left|\frac{dU_{LJ}\left(r_{ij}\right)}{dr_{ij}}\right|_{r=r_c} - |U_{LJ}\left(r_{ij}\right)|_{r=r_c} \tag{3}$$

with

$$U_{LJ}\left(r_{ij}\right) = 4\varepsilon\left[\left(\frac{\sigma}{r_{ij}}\right)^{12} - \left(\frac{\sigma}{r_{ij}}\right)^{6}\right] \tag{4}$$

where $\varepsilon (=1)$ is the potential-energy parameter and σ is the size of each site. Both chains and solvent have the same size in all sites. Notice that the molecular model used here is similar to those used in previous studies of associative polymers [35,38].

To maintain connectivity between the adjacent sites of a chain, the Lennard-Jones potential is used in conjunction with the FENE attractive potential:

$$U_{FENE}\left(r_{ij}\right) = -0.5 k_v R_0^2 \ln\left[1 - \left(\frac{r_{ij}}{R_0}\right)^2\right] \tag{5}$$

where $k_v (= 100)$ is the spring constant and $R_0 = (1.5\sigma)$ is the maximum length of the bond. It is known that the FENE potential adequately reproduces the behavior of polymeric solutions [49]. In polymer solutions, associative or unmodified, molecular sites along the chain and solvent molecules interact via attraction-repulsion modes according to the modified Lennard-Jones potential (Eqs. (3)–(4)). The FENE potential (Eq. (5)) accounts for the chemical bond between adjacent sites along the chain. In addition to these potentials, hydrophobic sites (HS) interact through an attractive potential to reproduce the association between them:

$$U_A\left(r_{ij}\right) = -\frac{\varepsilon_c}{r_{ij}}\left[1 - \left(\frac{r_{ij}}{r_c}\right)^2\right]^2 \tag{6}$$

where $\varepsilon_c (=5.4)$ is the potential-energy parameter, r_c is the cutting radius of the potential and r_{ij} is the scalar distance between hydrophobic sites. The attractive potential given by Eq. (6) is a short-ranged potential so it only applied for $r_{ij} \leq r_c$, considering that r_c is equal to 2.5σ. Note that the association force among the hydrophobic sites depends on the energy-parameter ε_c. In this

Table 1
Quantities expressed in Lennard-Jones reduced units.

Physical quantity	LJ unit	As a reference SI unit for CH_2
Length	σ	3.93×10^{-10} m
Mass	m	14 kg/kmol
Energy	ε	6.489×10^{-22} J
Number density	$1.0/\sigma^3$	16.47 nm^{-3}
Temperature	ε/k_B	47 K
Time	$(m\sigma^2/\varepsilon)^{1/2}$	2.35×10^{-12} s
Stress	ε/σ^3	10.69 MPa
Viscosity	$(m\varepsilon)^{1/2}/\sigma^2$	2.51×10^{-5} kg/m s
Shear rate	$(\varepsilon/m\sigma^2)^{1/2}$	4.25×10^{11} s^{-1}

work, it will be shown the crowding among the hydrophobic sites due to associations occurring for $\varepsilon_c = 5.4$.

2.3. Equations of motion

In the system, the position $\mathbf{r}_i^N$ and velocity $\mathbf{v}_i^N$ vectors of the particles evolve at constant volume and temperature, in which a Nose–Hoover thermostat is used [50]. The equations of motion under simple shear flow are [51]:

$$\frac{di\mathbf{r}}{dt} = i\mathbf{v} + i\mathbf{r} \cdot \nabla\mathbf{v} \tag{7}$$

$$\frac{di\mathbf{v}}{dt} = \frac{i}{m_i}\mathbf{F} - i\mathbf{v} \cdot \nabla\mathbf{v} - V_\xi i\mathbf{v} \tag{8}$$

$$\frac{dV_\xi}{dt} = \frac{1}{Q}\sum_i m_i v_i^2 - LT \tag{9}$$

where $\nabla\mathbf{v}$ is the velocity gradient, r_i and v_i are the position and peculiar velocity vectors of particle i; m_i and F_i are mass and force associated with particle i, whereas the force on particle i stems from the interactions expressed in Eqs. (2)–(6) among the system elements. Under simple shear, the flow-direction is x and the gradient and vorticity directions are z- and y, respectively. For steady shear flow, $v_x = \dot{\gamma}_{zx}z$, $v_y = v_z = 0$, such that, $\nabla\mathbf{u} = \dot{\gamma}i\mathbf{k}$, where, $\dot{\gamma}$ is the shear rate. In the Eqs. (8) and (9), Q is the mass associated to the thermostat and V_ξ its velocity coordinate. The mass of the thermostat is given by $Q = LT/\omega_p^2$ [52], where ω_p is the frequency at which the thermostat fluctuates and $L(=3N)$ is the number of degrees of freedom coupled to the thermostat. In this work, $1/\omega_p$ is equal to 0.01054; similar value used in previous shear flow simulations of polymer melts [53]. To keep the flow homogeneous, the solution of the equations of motion (7)–(9) is coupled to the Lees–Edwards periodic boundary conditions [54].

3. Details of the simulations

3.1. System units

All variables and system parameters are expressed in dimensionless (or reduced) units, normalized with respect to the characteristic Lennard-Jones parameters (energy ε, site-diameter σ) and the mass of each site m_i, with assigned values of $\varepsilon = \sigma = m_i = 1.0$. The dimensionless variables follow the corresponding-state principle. Table 1 shows the main normalized-variables of the simulations with conversion factors to obtain the real units (taking as a reference-site the CH_2 molecule) [47]. Note that as the molecular chain is represented according to the Kremer and Grest model [55] within the coarse-grain simulation scale, the reference site in the model is larger than the CH_2 site.

3.2. Conditions of simulations

The systems under study are composed of linear molecules in solution, wherein each molecule has 20 interlinked sites. The size of the system involves 8000 sites (sites of molecules and solvents) of σ size with a number density and reduced temperature of 1.0 and 1.5, respectively. The particles are contained in a cubic simulation region (side length equal to 20σ) whose origin is located in the middle of the flow domain. The concepts of periodic boundary condition and minimum image are applied in the three directions of the coordinate system.

The initial configuration used for flow condition is generated from equilibrium molecular-dynamics simulations, considering that the velocity gradient is zero. Once this configuration is obtained, a velocity gradient is applied in a range of shear-rates, i.e., $0.00005 \leq \dot{\gamma} \leq 0.2$. For shear-rates of the order of 0.001 and smaller, the duration of the simulations covers seven million integration steps, with $\Delta t = 0.001$, otherwise, the duration amounts to three million integration steps.

3.3. Calculation of the material properties

3.3.1. Material functions

Given a rectilinear Couette flow, the only non-zero component of the velocity vector is $v_x(z)$, with stress component σ_{zx}. For a simple shear flow, the viscosity η is given by:

$$\eta(\dot{\gamma}) = \frac{\langle\sigma_{zx}\rangle}{\dot{\gamma}} \tag{10}$$

where $\langle\sigma_{zx}\rangle$ is the average of the total shear stress:

$$\sigma_{zx} = -\frac{1}{V}[\langle\sum_i m_{zi} v_{zi} v_{xi}\rangle + \sum_i \sum_{ji} z_{ij} F_{xi}] \tag{11}$$

In Eq. (11), v_{xi} and v_{zi} are the peculiar velocities of particle i along flow and gradient directions, respectively, and V is the system-volume. Upon increasing the strain-rate, the polymer structure becomes anisotropic due to molecular alignment along the flow direction, which causes differences in the normal-stress components, inducing restoring elastic forces. These are:

$$<N_1> = \sigma_{xx} - \sigma_{zz} \tag{12}$$

$$<N_2> = \sigma_{zz} - \sigma_{yy} \tag{13}$$

3.3.2. Structure factor S(k)

The structural and conformational analysis of the solutions includes the calculation of structure factor $S(k)$, defined as the autocorrelation function $S(k) = 1/N\langle\rho_k\rho_{-k}\rangle$, where $\rho_k = \sum_{j=1}^{N} \exp{-i k \cdot \mathbf{r}_j}$ is the Fourier transform of microscopic density and r_j is the position vector of the particle j. For a cubic region of length L and total site number N, vector k is given by $2\pi L$, and so, its scalar components are restricted to multiples of $2\pi L$, as periodic boundary conditions are used. If k only has the components x and y, then:

$$\mathbf{k} = k_x\mathbf{i} + k_y\mathbf{j} = n_x\left(\frac{2\pi}{L}\right)\mathbf{i} + n_y\left(\frac{2\pi}{L}\right)\mathbf{j} \tag{14}$$

where n_x and n_y are integer numbers.

The structure factor can be measured experimentally using static light-scattering (SLS), which determines density fluctuations caused by light at wavelengths of $2\pi k$ [56]. Some of the properties that can be estimated from SLS experiments are the radius of gyration R_g, the average molecular weight M_w and the second virial coefficient B_2. The structure factor reveals the molecular conformation of associative polymers and their aggregates. Only position vectors of the chains are considered in the calculations.

3.4. Coordination number (n_c)

Aggregate formation is related to the density of hydrophobic associations and their topology. The degree of interactions among the different elements of the system is a function of the coordination number (n_c), which can be calculated from the radial distribution function of the hydrophobic groups $g_{HS}(r)$. The knowledge of n_c provides information on the first solvation-shell of a segment at a given distance r_m, which corresponds to the first minimum in $g_{HS}(r)$ appearing between the first and second peaks. Considering that the number of hydrophobic sites in the region of simulation is a continuous variable, the coordination number is given by:

$$n_c = \frac{N_{HS}}{V} 4\pi \int_0^{r_m} g_{HS}(r) r^2 dr \tag{15}$$

where N_{HS} is the number of hydrophobic sites in the system volume (V).

4. Results and discussion

4.1. Flow curves

Simple shear flow for telechelic, multi-sticker associative polymers and unmodified polymer solutions are performed at same conditions of density and reduced temperature, to elucidate the effect of the hydrophobic modification on the rheology of the system.

Viscosity $\eta(\dot{\gamma})$ of the unmodified-polymer solutions for different concentrations is shown in Fig. 2a. The concentrations per site of 0.0 and 1.0 (not included in the analysis) correspond to pure-solvent and pure-polymer (melt) conditions, respectively. The shear-viscosity (η) increases with solution concentration (c). At concentrations below 0.15, the system is Newtonian, with a plateau region of constant viscosity. At higher concentrations (0.15), the solution exhibits a Newtonian region followed by shear-thinning, starting at shear-rates of 0.005 with a slope of −0.31 at high concentrations ($c = 0.85$). Viscosity calculations for shear-rates of $\dot{\gamma} \leq 0.0005$ exhibit a considerable error, so results at very low shear-strains are not included. The error is estimated by the method of Flyvbjerg et al. [57]. The interplay between molecular interactions and molecular structure largely determines the rheological behavior of chain molecules. Since the region of shear-thinning is associated with alignment of polymer molecules in the flow direction, the density distribution of chain segments is increased in the direction of flow and decreases along the other two directions [58].

Comparison with the unmodified polymer solutions is shown in the flow curves of $\eta(\dot{\gamma})$ including the multi-sticker polymers (see Fig. 2b). A Newtonian behavior at low concentrations ($c = 0.04$) is observed. With increasing concentration, the systems exhibit two flow regions: a Newtonian followed by shear-thinning region with a slope of −0.5 for $c = 0.85$. This slope is larger than that of the unmodified polymer at the same concentration. With increasing concentration, shear-thinning appears at low shear-rates and without the presence of a thickening region. At $c = 0.85$, viscosity in the Newtonian region is approximately 10 times larger than its unmodified counterpart; however, both polymers have the same viscosity at high strains.

The variation of shear η as a function of shear rate $\dot{\gamma}$ for telechelic polymers is shown in Fig. 2c and d within the concentration ranges of $0.02 \leq c \leq 0.10$ and $0.15 \leq c \leq 0.85$, respectively. At very low concentrations ($c = 0.02$ y 0.04), the solutions show a Newtonian behavior followed by a shear-thickening region. For concentrations of 0.08 and 0.10, a shear-thinning region appears

following shear-thickening. Koga et al. [18] explain that the thickening is caused by the stretch experienced by bridge chains under shear-flow, and shear-thinning is caused by a break in the network aggregates. Both phenomena are analyzed in detail later.

When the solution has a concentration of 0.15 and 0.25, shear-thickening tends to disappear and the shear-thinning region sets in, exhibiting two slopes. For example, for c = 0.05, shear thinning has slopes of −0.54 and −0.15 at shear-rates of $0.0002 \leq \dot{\gamma} \leq 0.005$ and $0.005 \leq \dot{\gamma} \leq 0.2$, respectively. Sprakel et al. [10] report shear-thinning with two slopes in a solution of telechelic polymers in the semi-dilute entangled regime. Larger slopes are associated with non-homogeneous flows and vice versa. The two slopes in the shear-thinning region tend to disappear with increasing concentration, such that a single slope with a value of −0.66 at $c = 0.85$ is predicted, which contrasts with values of −0.50 and −0.31 in the case of their multi-stickers and unmodified counterparts, respectively.

4.2. Viscosity

In Fig. 2, flow curves $\eta(\dot{\gamma})$ are illustrated considering the three types of polymer solutions. Traditionally, viscosity η_0 is obtained by extrapolation to zero shear-rate viscosity in the first Newtonian region. However, in the case of associative polymer solutions, few statistically-reliable measurements were obtained. It is considered that η_0 is equivalent, as a first approximation, to the viscosity corresponding to the lower $\dot{\gamma}$ reached in the simulations. The curves of η_0 versus concentration are shown in Fig. 3.

The unmodified polymer solution comprised four concentration regimes [20,59]. (i) Dilute regime ($c < c^*$). In this regime the solution viscosity (η_0) is similar to that of the solvent. Since the viscosity of the solvent is 6.7 (obtained from molecular-dynamics simulations under simple shear flow), the first regime extends to a concentration of 0.08, wherein the viscosity of the solution is 7.3. Therefore, the concentration per site of 0.08 is considered as the overlap concentration (c^*). (ii) Semi-dilute unentangled regime ($c^* < c < c_e$). This regime extends up to the concentration of elastically-effective entanglements (c_e). The concentration c_e is obtained from that corresponding to the crossing of the extrapolated lines of dilute regime and semidilute entangled regime (rendering a value of $c_e = 0.20$). In this regime, the viscoelasticity of the solution is predicted by Rouse dynamics and the viscosity increases moderately; the power exponent is 0.25. (iii) Semi-dilute entangled regime ($c_e < c < c^{**}$). Jiménez-Regalado et al. [59] suggest that this regime extends up to the critical concentration c^{**}, where viscoelasticity of the solution evolves according to the Reptation model. Concentration c^{**} defines the beginning of the concentrated regime in which the volume fraction of the polymer is between 0.2 and 0.3 [60]. (iv) Concentrated regime ($c > c^{**}$). This is located above the critical concentration (c^{**}) and the Reptation model predicts the solution behavior. The critical concentration of the onset for the concentrated regime is not predicted here. Since the solutions are formed by chains of 20 sites (or segments), the dynamics is governed by the Rouse model. In this regard, the entanglement concentration c_e identifies the onset for chain-motion restrictions due to excluded volume effects, rather than topological entanglements.

In the case of the associative polymers, dilute and semi-dilute unentangled concentration regimes extend up to the concentrations c_η and c_T, respectively [22,59]. The concentration c_η corresponds to the viscosity of the associative polymer that exceeds the viscosity of the unmodified polymer and c_T is obtained by curve-extrapolation of the semi-dilute unentangled and entangled regimes.

As shown in Fig. 3, the viscosity of the telechelic polymers exceeds that of the unmodified at a concentration of 0.08, such that $c_\eta \cong 0.08$. Here, c_η of this associative polymer is similar to
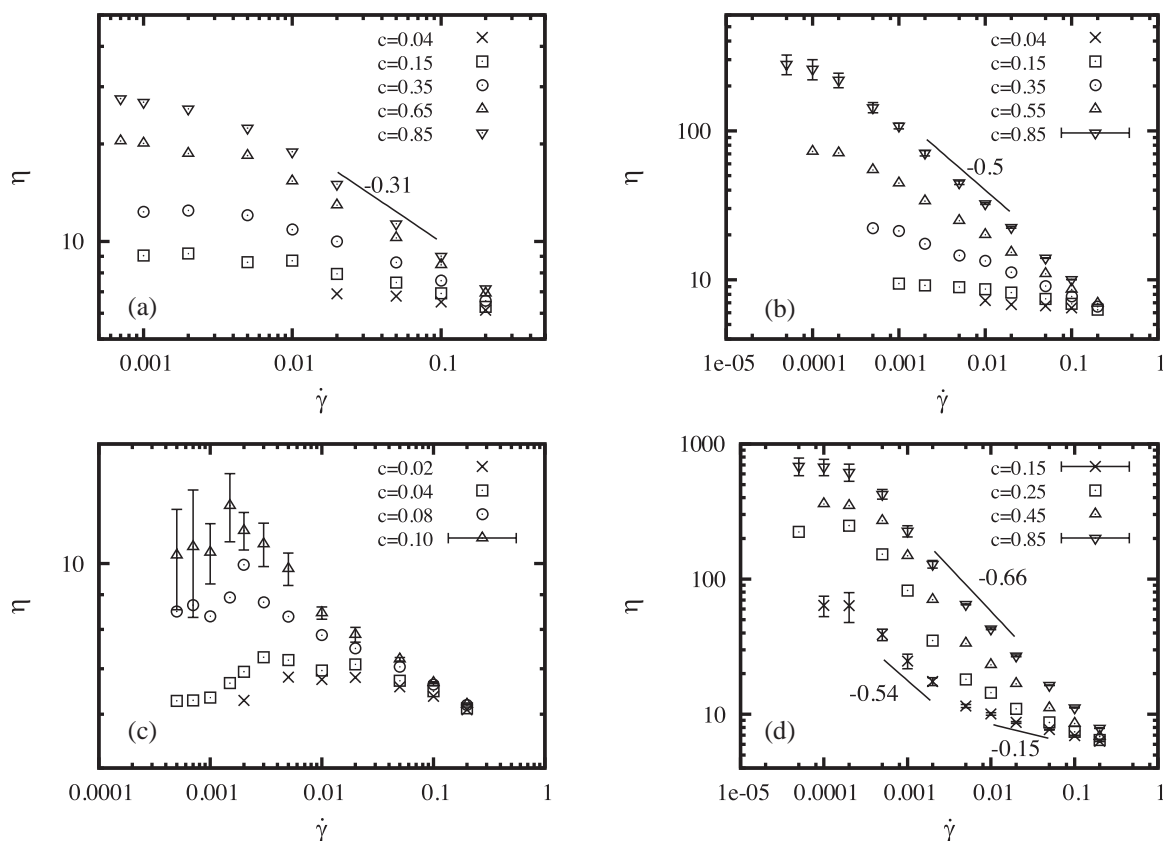
Fig. 2. Variation of shear viscosity (η) as a function of shear rate ($\dot{\gamma}$) for polymer solutions: (a) unmodified, (b) multi-sticker associative, and (c)–(d) telechelic associative.
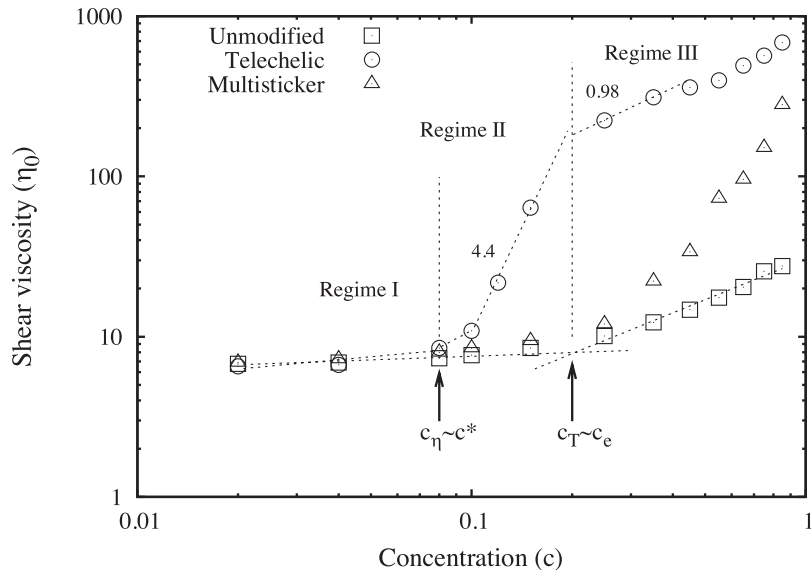

Fig. 3. Variation of shear viscosity at zero shear-rate (η_0) as a function of the concentration per site (c) for unmodified and associative polymer solutions.

c^*, inasmuch as the *dilute regime* ($c < c_\eta$) holds in the same range of concentrations for both polymers. In the case of associative multi-sticker polymer, c_η cannot be determined, since throughout the concentration range η_0 is higher than that of the unmodified polymer. For telechelic polymer solutions $c_T \cong 0.19$, such that $c_T \sim c_e$ and the semidilute unentangled regime lies in a similar concentration range of the unmodified polymer ($c_\eta < c < c_T$). In the latter regime, the telechelic polymer viscosity increases steeply, with a power exponent of 4.4; while in the multi-sticker poly-

mer, viscosity increases moderately with a slope alike to that of the unmodified polymer. Rubinstein et al. [9] predict an exponent of 5.9 for associative polymers in the second regime, considering a renormalization of the lifetime bonds between hydrophobic sites (HS), without which the exponent of the power would be 4.2. According to these authors, the slope exhibited by the telechelic polymers in the second regime indicates that two separated HS can always find another association with a third HS. In the *semi-dilute entangled regime* ($c_T < c < c^{**}$), the solution-viscosity increases moderately
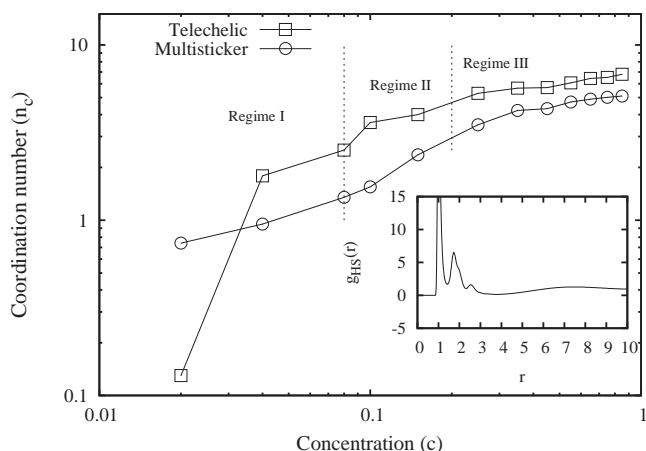
Fig. 4. Variation of coordination number (n_c) as a function of the concentration per site (c) for associative polymer solutions. In the inset, the radial distribution function ($g_{HS}(r)$) for a telechelic polymer ($c = 0.55$) is included.

with a slope (about 1.0) similar to that of the unmodified polymer. The value of the slope is consistent with that predicted by Rubinstein et al. for solutions that behave according to the Rouse model.

Numerous studies have reported that strong viscoelasticity of the associative polymers is evident from the semi-dilute unentangled regime and above the critical aggregation concentration [10,22]. However, in multi-sticker associative polymers the viscosity is slightly higher than its unmodified counterpart in this regime. The thickening effect of the hydrophobic groups in multi-sticker polymers, which deviate from the behavior of the unmodified polymers, is manifested above c_T, with a power exponent close to 3. A similar behavior has been observed in aqueous solutions of hydrophobically-modified polyacrylamides [22,59]. Cram et al. [22] indicate that the slope in the semi-dilute unentangled regime depends on the content and length of the hydrophobic groups.

4.3. Structural analysis

Once the concentration regimes of the solutions of unmodified and associative polymers are defined, the structural analysis allows determining the molecular origins of the solution-viscoelasticity within each concentration regime. The structure of the solutions is discussed in terms of the coordination number (n_c) and structure factor ($S(k)$). In addition, an analysis of the resulting configurations of the systems under study is included.

4.3.1. Coordination number (n_c) and radial distribution function ($g_{HS}(r)$).

The coordination number n_c as a function of concentration is shown in Fig. 4. In the inset, the radial distribution-function of the hydrophobic sites $g_{HS}(r)$ from which n_c is obtained, is shown. Radial distribution function $g_{HS}(r)$ of the *telechelic polymer* at $c = 0.55$ (within the concentrate regime) displays the structural arrangement exhibited by the hydrophobic sites in the domain of simulation. Function $g(r)$ of a simple liquid exhibits peaks at distances of 1σ, 2σ, 3σ, etc., where the peaks indicate the presence of first, second and third neighbors. In the case of *telechelic polymers*, $g_{HS}(r)$ exhibits a peak at a concentration of 0.02, two peaks in the range $0.04 \leq c \leq 0.25$, and three peaks at $c > 0.25$. Unlike simple liquids, $g_{HS}(r)$ exhibits three shells of first neighbors but at smaller separation distances (1σ, 1.7σ, 2.5σ), indicating a clumping of hydrophobic sites.

Radial distribution function $g_{HS}(r)$ of *solutions of telechelic polymers in the dilute regime* (not shown) reveals associations between

hydrophobic sites presumably corresponding to isolated chains, and for contents larger than $c = 0.04$, the two peaks indicate associations between hydrophobic sites of isolated chains and formation of micellar aggregates in the first three concentration-regimes. The existence of the third peak at a concentration of 0.35 suggests an increase in the number of hydrophobic sites that form the core of the micellar aggregates. In *solutions of multi-sticker polymers*, $g_{HS}(r)$ exhibits a peak in the *dilute regime* and formation of aggregates (due to the presence of two peaks) in the *semi-dilute unentangled regime*. These polymers do not exhibit three peaks, suggesting that the aggregate-cores contain smaller number of hydrophobic sites than the aggregate-cores in telechelic polymers. It is noteworthy that in both associative polymers, the first peak of $g_{HS}(r)$ decreases as c increases, suggesting a larger number of associations among hydrophobic sites in aggregate-cores and between hydrophobic sites of different aggregates.

Fig. 4 shows the coordination numbers (n_c) of both associative polymers in the whole concentration range. Since they do not exhibit the same number of peaks of the function $g_{HS}(r)$, n_c was obtained from the first peak ($r_m = 1.5\sigma$) corresponding to first hydrophobic-neighbors. In *multi-sticker polymers*, the behavior of n_c indicates the transition between concentration regimes. Since $n_c < 1.0$ in the *dilute regime*, a layer of first hydrophobic-neighbors is present, with transient associations between hydrophobic sites. In the *semi-dilute unentangled regime*, $n_c > 1.0$ indicates the existence of a permanent shell of first hydrophobic-neighbors, presumably due to the formation of aggregates with a core with reduced number of hydrophobic sites. The number of first hydrophobic-neighbors tends to remain constant with a value close to 5.0.

In *telechelic polymers*, $n_c = 0.12$ at a concentration of 0.02 (see Fig. 4), indicating absence of interactions between hydrophobic sites (HS); hence at this concentration these polymers exhibit the lower Newtonian viscosity (see Fig. 3). Upon increasing concentration, a permanent shell of first hydrophobic-neighbors larger than that of the multi-sticker polymers ($n_c \geq 0.2$) reveals stronger interactions among HS than its counterpart in the whole concentration range. The telechelic polymer topology allows larger HS interactions with larger zero shear-rate viscosity. In the transition from dilute to the semi-dilute unentangled regime, n_c suddenly increases from 2.5 to 3.6, remaining almost constant in the second regime. In the transition from the second to the third regime, n_c increases from 4.0 to 5.3, and exhibits values close to 7.0 at high concentrations. The nearly constant coordination number in the semi-dilute unentangled regime and at high concentration suggests an increase in the number of aggregates, but not in the number of chains of each aggregate.

4.3.2. Analysis of the final configurations

Fig. 5 shows the resulting configuration of *telechelic polymer solutions* at each concentration regime. In the *dilute regime* (Fig. 5a and b), molecules are isolated at very low concentrations ($c = 0.02$) with weak intra-chain interactions. In the same regime ($c = 0.04$) two aggregates of isolated micellar-flowers emerge. In the *semi-dilute unentangled regime* (Fig. 5c) a configuration in two dimensions corresponding to a concentration of 0.15 is shown. The configuration has six micellar-flowers (consisting of absorbed loops) with bridges between aggregates, dangling chains and one isolated chain. In this regime, it is likely that a balance between the intra and inter-chain associations exist (where each interacting HS acts as an effective friction-site) being proportional to the lifetime of the association [9]. Finally, in the *semi-dilute entangled regime* (Fig. 5d) it is likely that most of the molecules inter-act with each other, resulting in a configuration with visible cores, revealing an augmented number of aggregate and bridges between aggregates with respect to the previous regime. This configuration includes dangling chains but not isolated chains.
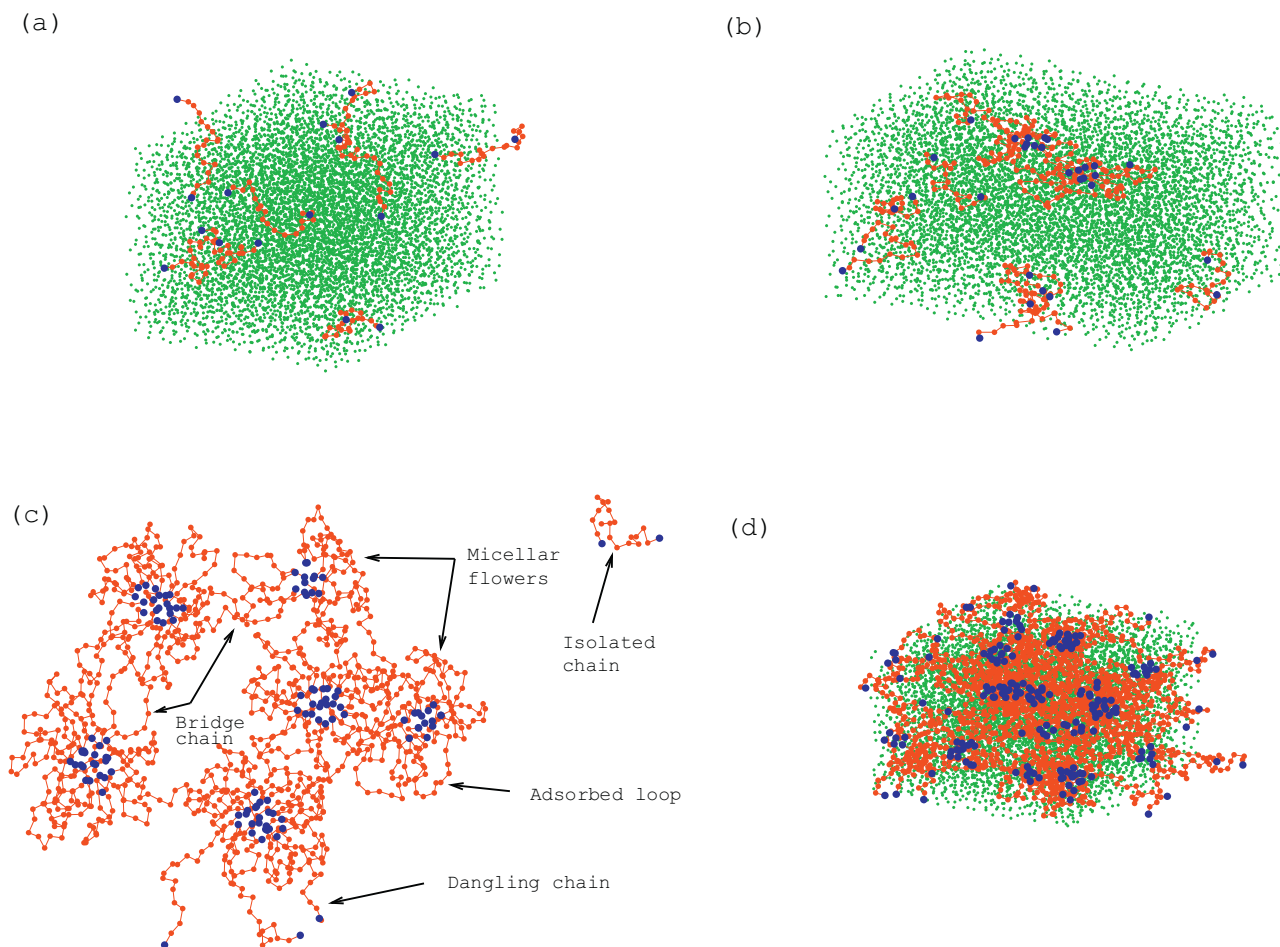
Fig. 5. Final configuration for a telechelic polymer solution at (a) $c = 0.02$, (b) $c = 0.04$, (c) $c = 0.15$, and (d) $c = 0.25$. Green dot (solvent particle), blue dot (hydrophobic site). Solvent particles are omitted for clarity in (c). (For interpretation of the references to color in this figure legend, the reader is referred to the web version of this article.)
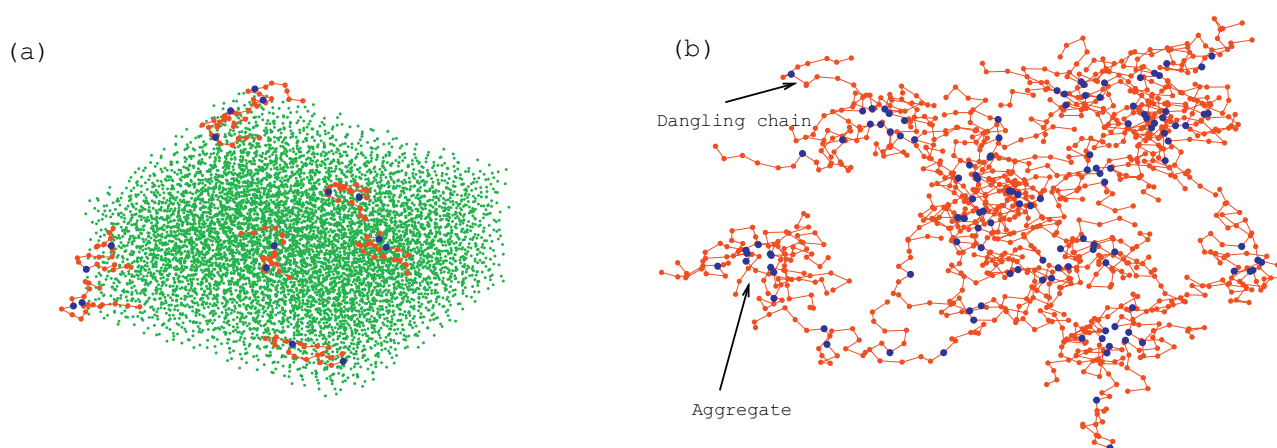

Fig. 6. Final configuration for multi-sticker associative polymer solution at (a) $c = 0.02$, (b) $c = 0.15$. Green dot (solvent particle), blue dot (hydrophobic site). Solvent particles are omitted for clarity in (b). (For interpretation of the references to color in this figure legend, the reader is referred to the web version of this article.)

In *multi-sticker polymers*, the resulting configurations at concentrations of 0.02 and 0.15 (corresponding to dilute and semi-dilute unentangled regimes) are presented in Fig. 6. In contrast to telechelic polymers, formation of aggregates is hard to visualize. In the *dilute regime*, the chains do not interact with each other since they are mostly isolated (see Fig. 6a). Since the hydrophobic sites are located in sites 7 and 14 of the chain, intra-chain interactions tend to flex the isolated molecule to form a kind of knot. In both sides of the knot, sites 8–13 form a closed loop and linked sites 1–6 and 15–20 form two tails. When the concentration increases, a set of knots can form an aggregate, as shown in Fig. 6b. Results of n_c demonstrate that the number of HS forming the core of the new aggregate is smaller than the HS in the core of the micellar flowers, presumably because of topological and motion constraints of the tails of each knot.
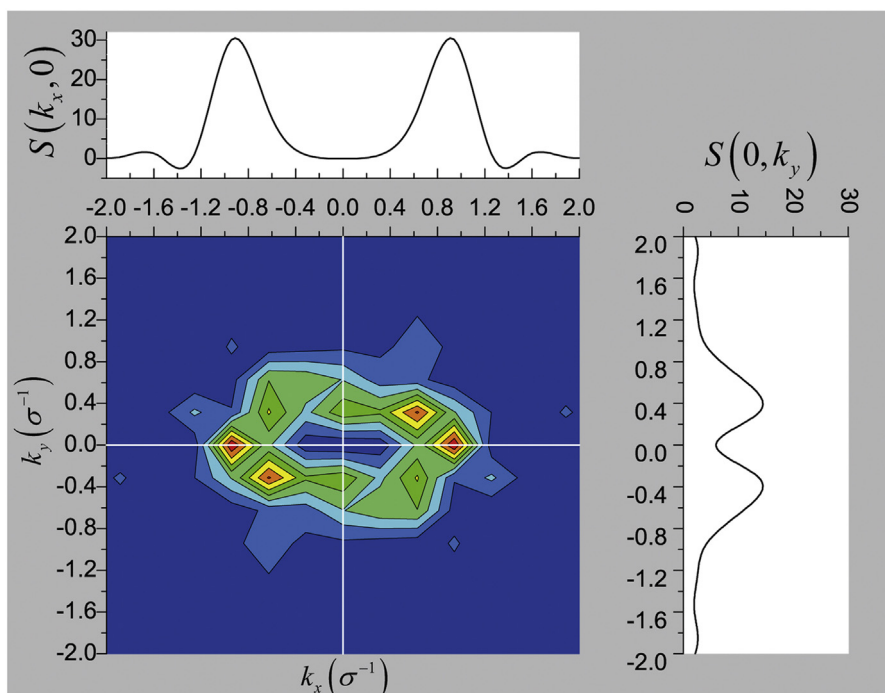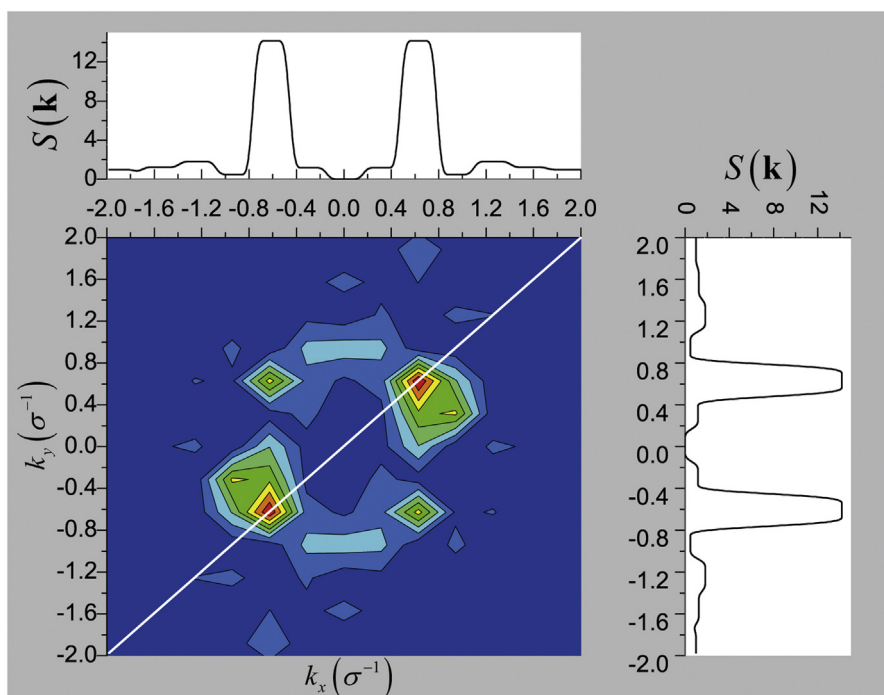
(a) Telechelic polymer
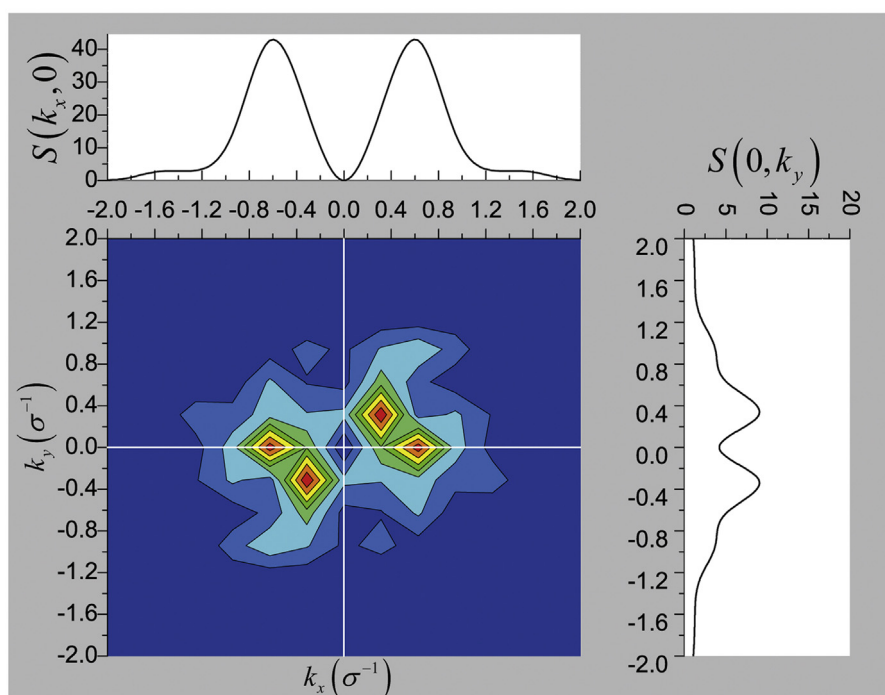
(b) Multi-sticker polymer

Fig. 7. Structure factor (S(k)) for associative polymer solutions in the semi-dilute unentangled regime (c = 0.15): (a) Telechelic, and (b) multi-sticker.
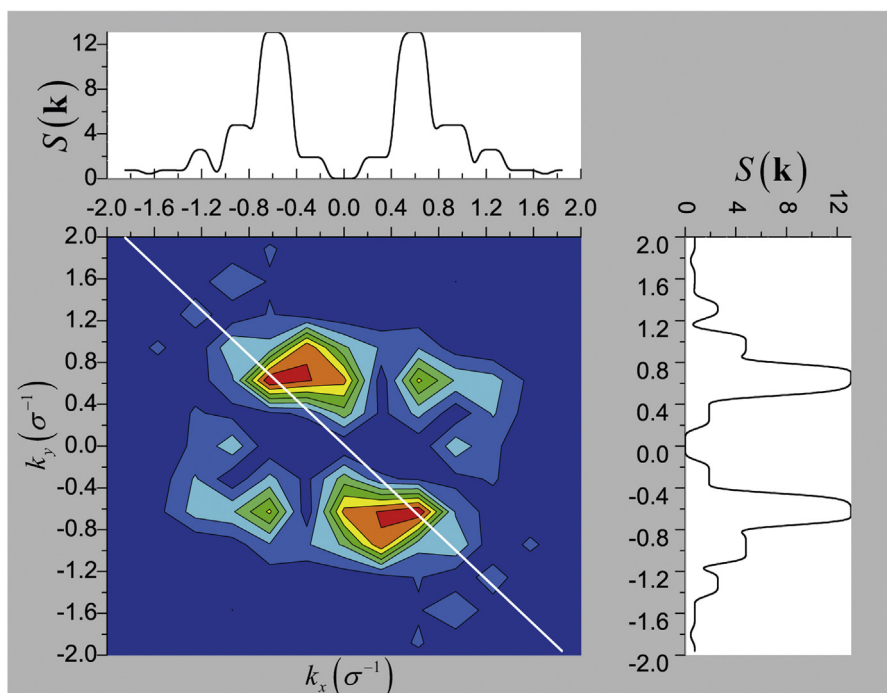
4.3.3. Structure factor

In Fig. 7 the static structure-factor of the associative polymers in the semi-dilute unentangled regime is exposed (for $c = 0.15$). In Fig. 7a, the telechelic polymers structure-factor contains four well-defined peaks suggesting polymer chains associated in micellar flowers (see Fig. 5c). Two peaks are positioned on the line at $k_y = 0$ with values of $S(k_x,0) = 30.11$ corresponding to $k_x \cong \pm 0.94$. These peaks tend to approach each other ($k_x \cong \pm 0.6$) while increasing intensity ($S(k_x) = 44.54$) in the multi-sticker case (see Fig. 7b). This incremental intensity suggests an increasing alignment of the multi-sticker polymer along the x-direction, revealing larger

(a) Telechelic polymer

(b) Multi-sticker polymer

Fig. 8. Structure factor (S(k)) for associative polymer solutions above the semi-dilute entangled regime (c = 0.55): (a) Telechelic, and (b) multi-sticker.

molecular mobility and lower viscosity than those of the telechelic polymers [56].

Above the semi-dilute unentangled regime (c = 0.55), the telechelic polymer exhibits four peaks (see Fig. 8a) two of them are weak and oriented at 135°, while two well-defined peaks are

located at 45° above the horizontal with values of $S(k_x, k_y) = 14.17$. The lower intensity respect to the second regime is associated to a large light absorption as the concentration increases [56].

The multi-sticker polymers also exhibit four peaks (see Fig. 8b), two of them are weak located at 45° and the other two are well-
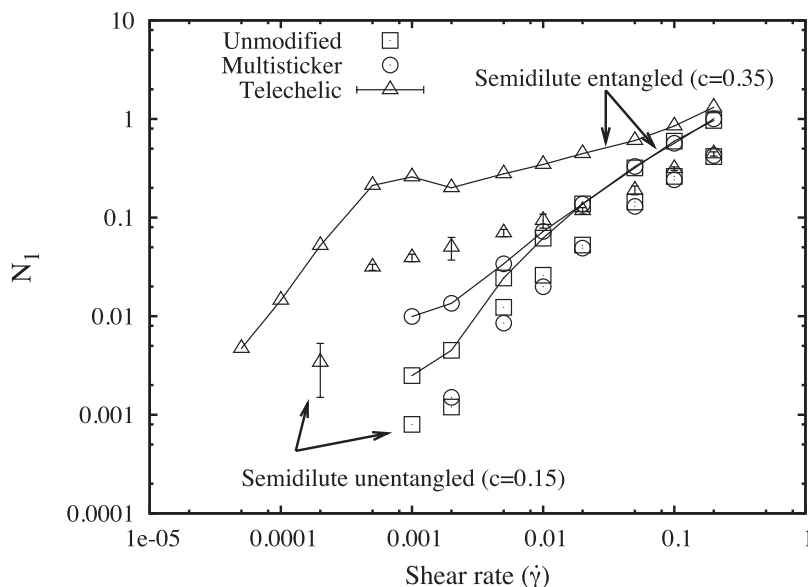
Fig. 9. First normal stress difference (N_1) as a function of shear rate ($\dot{\gamma}$) for unmodified and associative polymer solutions, at $c = 0.15$ (points) and $c = 0.35$ (lines-points).

defined with values of $S(k_x, k_y) = 13.08$ located at 135°. Notice that the weak peaks in the telechelic polymer evolve into well-defined peaks in the multi-sticker polymer and viceversa, suggesting similar ordering of the aggregates but positioned at different regions of the simulation box. The observed wider peaks in the multi-sticker polymer implies a structure with a degree of isotropy, which may be explains the slope corresponding to the third regime of the viscosity variation with concentration ($\eta_0(c)$).

4.4. Other material functions

Results of the first normal-stress difference (N_1) corresponding to the second and third concentration regimes are presented. N_1 signals the presence of a non-isotropic configuration related to the elasticity under shear-flow. It is expected that the position of the hydrophobic sites in the chain have an effect upon the elasticity of the solution.

The variation of the first normal-stress difference (N_1) as a function of shear rate ($\dot{\gamma}$) for the three solutions (at concentrations of 0.15 and 0.35 corresponding to semi-dilute unentangled and entangled regimes) is presented in Fig. 9. In the second regime, results of the multi-sticker polymer show no difference with the unmodified polymer, indicating that the hydrophobic groups have a weak effect on polymer conformation. At low rate of strain ($\dot{\gamma} = 0.001$), N_1 of the telechelic polymer is almost two orders of magnitude larger than of the reference polymer, revealing a highly- elastic non-isotropic structure. A similar behavior is observed in the semi-dilute entangled regime ($c = 0.35$), along which the telechelic polymer exhibits the larger N_1 associated to an elastic network (see Fig. 5d). In the semi-dilute entangled regime, the hydrophobic associations of the multi-sticker polymer are strong enough, and hence possessing larger elasticity than that of the unmodified reference polymer at low shear-rates.

5. Conclusions

In this work, molecular-dynamics simulations are employed to describe the effect of hydrophobic groups on the rheological behavior of telechelic and multi-sticker associative polymer solutions with respect to that of the reference, unmodified polymers. The polymer molecules are represented according to the Kremer and Grest model [55] within a coarse-grain simulation scale. An attrac-

tive potential is included to reproduce the interactions between hydrophobic sites. A simple shear flow is generated by solving the equations of motion under the *NVT* ensemble and *SLLOD* dynamics [51], where a Nose–Hoover thermostat is used to maintain a constant temperature.

Three concentration regimes are identified: (1) dilute, (2) semi-dilute unentangled and (3) semi-dilute entangled. Simulations were performed within a wide concentration range per site, and transitions among the concentration regimes are common to modified and unmodified polymers. In the *dilute regime*, the multi-sticker polymer exhibits a Newtonian region of constant viscosity contrasting with the behavior exhibited by telechelic polymers, where the Newtonian region is followed by shear thickening. A structural analysis reveals the presence of a transient first-layer of hydrophobic neighbors, which is associated with the viscosity of the associative polymer. The configuration at long times indicates that the molecules are isolated, so that the majority of hydrophobic interactions occur between sites of the same chain. In this regime, molecular conformation depends on the type of polymer; in the telechelic polymers, molecules form closed and/or open loops, while in the multi-sticker case, molecules tend to form knots.

In the *unentangled semi-dilute regime*, both associative polymers exhibit a Newtonian region followed by shear thinning; the thickening exhibited by the telechelic polymers in the dilute regime tends to disappear in this regime. Newtonian viscosity of the multi-sticker polymer is slightly higher than that of the unmodified polymer, while the telechelic ones experience a sudden increase with a slope of 4.4. According to the Rubinstein et al. theory [9], the slope indicates that two separated hydrophobic sites can always find another association with a third site. In this regime, the associative polymers form aggregates, where the amount of hydrophobic sites in the core is larger in the telechelic polymers. The configuration of the telechelic polymer reveals micellar flowers connected by bridges, where a flower is formed by a collection of closed loops. At low shear-rates, the connection between aggregates generates a non-isotropic structure with an elasticity level of almost two-orders of magnitude larger than that of the unmodified polymer. The static structure factor suggests an increasing alignment of the multi-sticker polymer along the *x*-direction, revealing larger molecular mobility and lower viscosity than those of the telechelic polymers.

In the *entangled semi-dilute regime* and even at high concentrations, the viscosity of the associative polymers in Newtonian region is considerably larger than that of their unmodified counterparts, such that the shear-thinning region exhibits a slope two-fold larger at high concentrations. At large shear-rates, the three polymers tend to similar shear-viscosity values. Both associative polymers exhibit a permanent shell of first hydrophobic neighbors indicating the presence of aggregates. In the case of the telechelic polymers, these aggregates constitute a highly elastic network, without the presence of isolated chains.

Finally, these results reveal that the hydrophobic groups and their position in the molecule have a strong influence upon the viscoelastic behavior of associative polymers. In the telechelic case, their influence is observed even within the dilute regime (aggregates formation with connections among them which induces increasing viscosity and elasticity at low shear-rates). When the hydrophobic groups are located along the molecule contour, topological constraints restrict the hydrophobic interactions, and the thickening appears only within the third regime.

Acknowledgments

References

[1] J.G. Hernández Cifre, T.M.A.O.M. Baredrug, J.D. Schieber, B.H.A.A. van den Brule, Brownian dynamics simulations of reversible polymer networks under shear using a non-interacting dumbbell model, J. Non-Newton. Fluid Mech. 113 (2003) 73–96.
[2] K. Persson, P.C. Griffiths, P. Stilbs, Self-diffusion coefficient distributions in solutions containing hydrophobically modified water-soluble polymers and surfactants, Polymer 37 (1996) 253–261.
[3] Y. Feng, P. Luo, C. Luo, Q. Yan, Direct visualization of microstructures in hydrophobically modified polyacrylamide aqueous solution by environment scanning electron microscopy, Polym. Int. 51 (2002) 931–947.
[4] F. Tanaka, T. Koga, Intramolecular and intermolecular association in thermoreversible gelation of hydrophobically modified associating polymers, Comput. Theor. Polym. Sci. 10 (2000) 259–267.
[5] M.A. Winnik, A. Yekta, Associative polymers in aqueous solution, Curr. Opin. Colloid Interface Sci. 2 (1997) 424–436.
[6] A. Tripathi, K.M. Tam, G.H. McKinley, Rheology and dynamics associative polymers in shear and extension: theory and experiments, Macromolecules 39 (2006) 1981–1999.
[7] L. Pellens, K.H. Ahn, S.J. Lee, J. Mewis, Evolution of a transient network model for telechelic associative polymers, J. Non-Newton. Fluid Mech. 121 (2004) 87–100.
[8] C. Chassenieux, T. Nicolai, L. Benyahia, Rheology of associative polymer solutions, Curr. Opin. Colloid Interface Sci. 16 (2011) 18–26.
[9] M. Rubinstein, A.N. Semenov, Dynamics of entangled solutions of associating polymers, Macromolecules 34 (2001) 1058–1068.
[10] J. Sprakel, E. Spruijt, M.A. Cohen Stuart, N.A.M. Besseling, M.P. Lettinga, J. van der Gucht, Shear banding and rheochaos in associative polymers networks, Soft Matter 4 (2008) 1696–1705.
[11] K.C. Tam, R.D. Jenkins, M.A. Winnik, D.R. Bassett, A structural model of hydrophobically modified urethane-Ethoxylate (HEUR) associative polymers in shear flows, Macromolecules 31 (1998) 4149–4159.
[12] R.D. Jenkins, The Fundamental Thickening Mechanism of Associative Polymers in Latex System: A Rheological Study, Ph.D., Chemical Engineering, Lehigh University, Lehigh, Pennsylvania, 1990.
[13] T. Annable, R. Buscall, R. Ettelaie, D. Whittlestone, The rheology of solutions of associating polymers comparison of experimental behavior with transient network theory, J. Rheol. 37 (1993) 695–726.
[14] W.K. Ng, K.C. Tam, R.D. Jenkins, Lifetime and network relaxation time of a heur-c20 associative polymer system, J. Rheol. 44 (2000) 137–147.
[15] B. Xu, A. Yekta, L. Li, Z. Masoumi, M.A. Winnik, The functionality of associative polymer networks: The association behavior of hydrophobically modified urethane-ethoxylate (heur) associative polymers in aqueous solution, Colloids Surf. A 112 (1996) 239–250.
[16] J. Mewis, B. Kaffashi, J. Vermant, R.J. Butera, Determining relaxation modes in flowing associative polymers using superposition flows, Macromolecules 34 (2001) 1376–1383.
[17] T. Indei, Necessary conditions for shear thickening in associating polymer networks, J. Non-Newton. Fluid Mech. 141 (2007) 18–42.
[18] T. Koga, F. Tanaka, Molecular origin of shear thickening in transient polymer networks: a molecular dynamics study, Eur. Phys. J. E 17 (2005) 115–118.
[19] G. Marrucci, S. Bhargava, S.L. Cooper, Models of shear-thickening behavior in physically cross-linked networks, Macromolecules 26 (1993) 6483–6488.
[20] E. Jiménez-Regalado, J. Selb, F. Candau, Viscoelastic behavior of semidilute solutions of multisticker polymer chains, Macromolecules 32 (1999) 8580–8588.
[21] P. Kujawa, A. Audibert-Hayet, J. Selb, F. Candau, Effect of ionic strength on the rheological properties of multisticker associative polyelectrolytes, Macromolecules 39 (2006) 384–392.
[22] S.L. Cram, H.R. Brown, G.M. Spinks, D. Hourde, C. Creton, Hydrophobically modified dimethylacrylamide synthesis and rheological behavior, Macromolecules 38 (2005) 2981–2989.
[23] F. Candau, E. Jimenez-Regalado, J. Selb, Scaling behavior of the zero shear viscosity of hydrophobically modified poly(acrylamides), Macromolecules 31 (1998) 5550–5552.
[24] L. Leibler, M. Rubinstein, R.H. Colby, Dynamics of reversible networks, Macromolecules 24 (1991) 4701–4707.
[25] M.R. Caputo, J. Selb, F. Candau, Effect of temperature on the viscoelastic behavior of entangled solutions of multisticker associating polyacrylamides, Polymer 45 (2004) 231–240.
[26] L. Pellens, R. Gamez Corrales, J. Mewis, General nonlinear rheological behavior of associative polymers, J. Rheol. 48 (2004) 379–439.
[27] W.K. Ng, K.C. Tam, R.D. Jenkins, Rheological properties of methacrylic acid/ethyl acrylate copolymer: comparison between an unmodified and hydrophobically modified system, Polymer 42 (2001) 249–259.
[28] C. Heitz, S. Pendharkar, R.K. Prud'homme, J. Kohn, A new strictly alternating comblike amphiphilic polymer based on peg. Part I: synthesis and associative behavior of a low molecular weight sample, Macromolecules 32 (1999) 6652–6657.
[29] C. Heitz, R.K. Prud'homme, J. Kohn, A new strictly alternating comblike amphiphilic polymer based on peg. Part II: associative behavior of a high molecular weight sample and interaction with sds, Macromolecules. 32 (1999) 6658–6667.
[30] A. Chakrabarti, R. Toral, Computer simulation of the aggregation process in self-associating polymer and surfact systems, J. Chem. Phys. 91 (1989) 5687.
[31] M. Kröger, R. Makhloufi, Wormlike micelles under shear flow: a microscopic model studied by nonequilibrium-molecular dynamics computer simulations, Phys. Rev. E 53 (1996) 2531.
[32] W.K. den Otter, S.A. Shkulipa, W.J. Briels, Buckling and persistence length of an amphiphilic worm from molecular dynamics simulations, J. Chem. Phys. 119 (2003) 2363–2368.
[33] J. Castillo-Tejas, J.F.J. Alvarado, S. Carro, F. Pérez-Villaseñor, F. Bautista, O. Manero, Rheology of wormlike micelles from non-equilibrium molecular dynamics, J. Non-Newton. Fluid Mech. 166 (2011) 194–207.
[34] P.G. Khalatur, A.R. Khokhlov, J.N. Kovalenko, D.A. Mologin, Molecular dynamics study of the solution of semiflexible telechelic polymer chains with strongly associating end groups, J. Chem. Phys. 110 (1999) 6039.
[35] D. Bedrov, G. Smith, J.F. Douglas, Structural and dynamic heterogeneity in a telechelic polymer solution, Polymer 45 (2004) 3961–3966.
[36] C. Ayyagari, D. Bedrov, G.D. Smith, Equilibrium sampling of self-associating polymer solutions: a parallel selective tempering approach, J. Chem. Phys. 123 (2005) 124912.
[37] F. Lo Verso, C.N. Likos, H. Löwen, Computer simulation of thermally sensitive telechelic star polymers, J. Phys. Chem. C 111 (2007) 15803–15810.
[38] C. Ayyagari, D. Bedrov, G.D. Smith, A molecular dynamics simulation study of the influence of free surfaces on the morphology of self-associating polymers, Polymer 45 (2004) 4549–4558.
[39] G. Brown, A. Chakrabarti, Structure formation in self-associating polymer and surfactant systems, J. Chem. Phys. 96 (1992) 3251.
[40] L. Huang, X. He, L. Huang, H. Liang, Computer simulation of the self-assembly of associating polymers, Polymers 44 (2003) 1967–1972.
[41] W. Carl, R. Makhloufi, M. Kröguer, On the shape and rheology of linear micelles in dilute solutions, J. Phys. II France 7 (1997) 931–946.
[42] P.G. Khalatur, A.R. Khokhlov, D.A. Mologin, Simulation of self-associating polymer systems. I. Shear-induced structural changes, J. Chem. Phys. 109 (1998) 9602.
[43] C. Manassero, C. Castellano, Telechelic melt polymer's structure variation depending on shear deformation, J. Macromol. Sci. Phys. 52 (10) (2013) 1465–1477.
[44] P.G. Khalatur, A.R. Khokhlov, D.A. Mologin, Simulation of self-associating polymer systems. II. Rheological properties, J. Chem. Phys. 109 (1998) 9614.
[45] P.G. Khalatur, D.A. Mologin, Rheological properties of self-associating polymer systems: nonequilibrium molecular dynamics simulation, J. Mol. Liq. 91 (2001) 205–217.
[46] M.J. Cass, D.M. Heyes, R.-L. Blanchard, R.J. English, Simulations and experiments of self-associating telechelic polymer solutions, J. Phys. Condens. Matter 20 (2008) 335103.
[47] J. Castillo-Tejas, S. Carro, O. Manero, Elastic response from pressure drop measurements through planar contraction–expansion geometries by molecular dynamics: structural effects in melts and molecular origin of excess pressure drop, Rheol. Acta 52 (2013) 767–783.
[48] B. Busic, J. Koplik, J.R. Banavar, Molecular dynamics simulation of liquid bridge extensional flows, J. Non-Newton. Fluid Mech. 109 (2003) 51–89.
[49] R. Bird, C. Curtiss, R. Armstrong, O. Hassager, Dynamics of polymeric liquids Kinetic Theory, vol. II, Wiley Interscience, New York, 1987.

[50] S. Nose, A unified formulation of the constant temperature molecular dynamics methods, J. Chem. Phys. 81 (1984) 511–519.

[51] D. Evans, G. Morriss, Statistical Mechanics of Non-equilibrium Liquids, Academic Press, New York, 1990.

[52] G.J. Martyna, M.E. Tuckerman, D.J. Tobias, M.L. Klein, Explicit reversible integrators for extended systems dynamics, Mol. Phys. 87 (1996) 1117–1157.

[53] Z. Xu, J.J. de Pablo, S. Kim, Transport properties of polymer melts from nonequilibrium molecular dynamics, J. Chem. Phys. 102 (1995) 5836–5844.

[54] A.W. Lees, S.F. Edwards, The computer study of transport processes under extreme conditions, J. Phys. C 5 (1972) 1921–1928.

[55] K. Kremer, G. Grest, Dynamics of entangled linear polymer melts: a molecular dynamics simulation, J. Chem. Phys. 92 (1990) 5057–5086.

[56] E.O. Castrejón-González, J. Castillo-Tejas, O. Manero, J.F.J. Alvarado, Structure factor and rheology of chain molecules from molecular dynamics, J. Chem. Phys. 138 (2013) 184901, 1-11.

[57] H. Flyvbjerg, H.C. Petersen, Error estimates on averages of correlated data, J. Chem. Phys. 91 (1989) 461–466.

[58] J. Castillo-Tejas, J.F.J. Alvarado, G. González-Alatorre, G. Luna-Barcenas, I.C. Sanchez, R. Macias-Salinas, O. Manero, Nonequilibrium molecular dynamics of the rheological and structural properties of linear and branched chain molecules. Simple shear and Poiseuille flow, instabilities and slip, J. Chem. Phys. 123 (2005) 054907.

[59] E. Jiménez-Regalado, G. Cadenas-Pliego, M. Pérez-Álvarez, Y. Hernández-Valdez, Study of three different families of water-soluble copolymers: synthesis, characterization and viscoelastic behavior of semidilute solutions of polymers prepared by solution polymerization, Polymer 45 (2004) 1993–2000.

[60] I. Teraoka, Polymer solutions, in: An Introduction to Physical Properties, John Wiley & Sons, New York, 2002.